Geomechanics and Engineering, *Vol. 27, No. 2 (2021) 151-165*
https://doi.org/10.12989/gae.2021.27.2.151

Comparative effects of adjacent loaded pile row on existing tunnel by 2D and 3D simulation models

Narunat Heama[1], Pornkasem Jongpradist*[2], Prateep Lueprasert[1], Suchatvee Suwansawat[1] and Pitthaya Jamsawang[3]

[1]*Department of Civil Engineering, School of Engineering, King Mongkut's Institute of Technology Ladkrabang, Bangkok, Thailand*
[2]*Construction Innovations and Future Infrastructures Research Center, Department of Civil Engineering, Faculty of Engineering, King Mongkut's University of Technology Thonburi, Bangkok, Thailand*
[3]*Soil Engineering Research Center, Department of Civil Engineering, King Mongkut's University of Technology North Bangkok, Thailand*

(Received March 11, 2021, Revised June 5, 2021, Accepted October 6, 2021)

Abstract. Selecting suitable simulation methods for complex problems requires a careful balance between the predicted accuracy and computational effort. This research comparatively investigated the effects of adjacent loaded pile row on an existing tunnel in terms of tunnel deformation and lining force, displacement of soil surrounding between tunnel and pile and load transfer of the pile. Simulations were carried out by eight simulation models consisting of 3D finite element (FE) full models (model 1-2); 3D FE symmetry models (model 3-4); and a pile wall in 2D FE models (models 5-8). In loaded pile row simulation, simulations were performed with two pile types: volume pile and embedded pile. In 2D simulation, the 3D pile row was converted into 2D pile wall under plane strain condition by using three transformation methods. The results show that the predicted tunnel responses are adequately accurate as long as the reasonable soil movement behavior can be reproduced. The 2D equivalent dimensions and 2D equivalent axial rigidity are recommended since they provide conservative estimation on both tunnel deformation and lining forces. The 2D equivalent flexural rigidity is not recommended if the pile response is also of concern. The novelty of this research lies in the use and discussion on the applicability of various 2D and 3D models to simulate the effects of adjacent loaded pile row on the existing tunnel, as opposed to previous studies which focused on one or two simulation models.

Keywords: 2D Finite element method; 3D Finite element method; adjacent loaded pile row; existing tunnel; tunnel response

1. Introduction

To make full use of limited ground space, major cities around the globe resort to underground tunnels for inner-city public rail transportation. With ongoing rapid urbanization, new infrastructure projects are constructed to accommodate population growth, including elevated roads, flyover, building complex. These new structures require pile foundations, especially in the soft ground area. As a result, the loaded piles of new structures are located adjacent to the existing tunnel. The adjacent loaded piles induce soil displacement, which in turn exacerbates tunnel deformation and lining force (Lueprasert *et al.* 2017a, Schroeder *et al.* 2004, Yan *et al.* 2006), reducing the bearing capacity and serviceability of the tunnels. It is thus of vital importance to investigate the effects of adjacent loaded piles on existing tunnels.

Finite element analysis (FEA) is commonly used to model the tunnel problem (Chen and Lee 2020, Djelloul *et al*. 2018, Heama *et al.* 2017, Yoo and Choi 2018). The 3D FEA was utilized to study the relationship between loaded piles and tunneling, given the 3D nature of tunneling (Jeon *et al.* 2020, Jongpradist *et al.* 2013, Nematollahi and Dias 2019, Zhang *et al.* 2018). The 3D FEA modeling requires large computational resources. As a result, 2D FE simulation models combined with some additional assumptions are preferably adopted (Schroeder *et al.* 2004, Yan *et al.* 2006). For example, a 3D pile row was converted into a 2D pile wall under plane strain condition considering equivalent dimension in previous studies on the effect of pile row on the nearby tunnel (Schroeder *et al.* 2004). In Schroeder *et al.* (2004), similar soil displacement and vertical stress in the soil surrounding the piles (without the existence of tunnel) were obtained from 2D and 3D FE models. The conversion of 3D pile row to 2D pile wall was thus adopted for subsequent analyses of tunnel response due to pile row under loading. However, the impact on the existing tunnel (i.e., tunnel deformation and lining forces) due to adjacent loaded pile row obtained from 2D and 3D FEA has never been directly compared. As a result, the applicability of 2D models for this situation is still questionable. In analyses of embankments supported by deep cement mixing piles, 3D pile rows were converted into 2D pile walls under plane strain condition (Chai *et al.* 2015, Jamsawang *et al.* 2019, Wijerathna and Liyanapathirana 2018) by various conversion methods and the analysis results were compared. Some shortcomings of 2D models

*Corresponding author, Associate Professor
E-mail: pornkasem.jon@kmtt.ac.th

ISSN: 2005-307X (Print), 2092-6219 (Online)

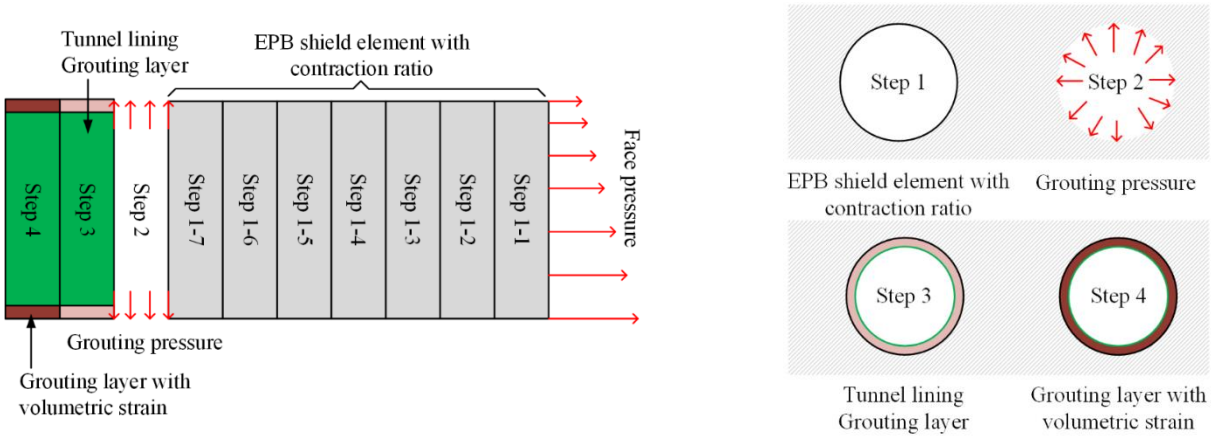

(a) 3D full models (models 1-2) (b) 3D symmetry (models 3-4) and 2D models (models 5-8)

Fig. 1 The tunneling simulation

have been revealed from their studies. Therefore, for the pile-soil-tunnel interaction problem, which is more complex, a better understanding of the applicability of 2D models is necessary.

The piles are commonly modeled using solid elements (volume pile). To reduce the complexity of numerical models, embedded pile formulation has been proposed and recently used in many applications. The embedded pile can provide similar pile head settlement and normal force along pile length (Sluis *et al.* 2014, Tschuchnigg and Schweiger 2015). To the best of our knowledge, there exists no research that compared the embedded pile and volume pile in the pile-soil-tunnel interaction problems.

Specifically, this research comparatively investigates the effect of an adjacent loaded pile row on an existing tunnel in terms of tunnel deformation and lining forces (i.e., bending moment and axial force). The behavior of adjacent loaded pile row included pile head settlement and normal force along pile length. The simulations were carried out by 2D and 3D FE models. There were eight simulation models: 3D finite element (FE) full models with volume pile (model 1) and embedded pile (model 2); 3D FE symmetry models with volume pile (model 3) and embedded pile (model 4); and a pile wall in 2D FE models with volume pile (models 5-7) and embedded pile (model 8). The accuracy and applicability of simulation methods in comparison to the 3D full model with volume pile were discussed and highlighted.

2. 3D and 2D FE simulation: Concepts, assumptions, and limitations

The 2D and 3D simulations of both tunneling and pile under loading need careful consideration so that their calculated tunnel deformation and lining forces can be reasonably comparable. For pile-soil-tunnel interaction, Lueprasert *et al.* (2017a) reveals that the mechanisms behind the tunnel deformation due to an adjacent loaded pile are principally due to the movement behavior of soil surrounding the tunnel, which in turn is dependent on the load transfer behavior from the pile. Therefore, each analysis model (a combination of tunneling simulation and simulation of loaded pile) must be carefully considered on the basis that it reproduces the similar soil movement behavior.

In this research, the continuous lining was used to simulate the tunnel lining. Although the tunnel lining is segmental in practice, continuous lining is considered to be sufficient for investigation on the lining structural forces of shallow tunnel (Klappers *et al.* 2006, Michael *et al.* 2016).

2.1 Tunneling simulation

In tunneling, the responses of surrounding soil and tunnel lining are subject to several tunneling factors, such as face pressure, grouting pressure, pitching angle, and penetration rate. Some factors cannot be considered in the 2D analysis, such as the face pressure. The numbers of tunneling parameters in the 3D full (models 1-2), 3D symmetry models (models 3-4), and the 2D simulation models (models 5-8) were unequal. In this study, tunneling simulations were carried out using the contraction method in Plaxis 2D and 3D software version 2018 using the measured data of tunneling factors that can be inputted. The contraction method is commonly used to simulate the effect of volume loss in tunneling (Lueprasert *et al.* 2017b, Vermeer and Brinkgreve 1993).

The tunneling parameters of 3D full models (models 1-2) included contraction ratio (CR), face pressure, grouting pressure, and volumetric strain (VS), while those of the 3D symmetry (models 3-4) and 2D models (models 5-8) were CR, grouting pressure, and VS. The contraction ratio (CR) is a percentage of area loss around a tunnel lining or a volume loss in the region of tunnel, which is expressed in Eq. (1).

$$CR=\frac{\text{(original tunnel area-tunnel area at current step)}}{\text{original tunnel area}} \quad (1)$$

The volumetric strain (VS) is the volume change of the harden grout, i.e., the change in volume divided by the original volume. In 2D FEA, the VS consists of two strain components (x- and z-directions), while in 3D FEA, there

Table 1 The 3D and 2D FE simulation models under study

Model	Description	Characteristic
1	3D full model with volume pile	Full-scale 3D model
2	3D full model with embedded pile	Full-scale 3D model
3	3D symmetry model with volume pile	Macro: plane strain with 3D pile
4	3D symmetry model with embedded pile	Macro: plane strain with 3D pile
5	2D model using equivalent dimensions	Plane strain
6	2D model using equivalent axial rigidity	Plane strain
7	2D model using equivalent flexural rigidity	Plane strain
8	2D model with embedded pile	Plane strain

Table 2 Parameters for soil layer of 3D and 2D simulation models

Layer	1	2	3	4	5	6	7	8
Soil type	Made Ground	Soft Clay	Medium Clay	1st Stiff Clay	1st Clayey Sand	2nd Stiff Clay	Hard Clay	2nd Clayey Sand
γ_{soil} (kN/m^3)	18	16.5	17.5	19.5	19	20	20	20
c' (kPa)	1	5	15	25	0	30	40	0
$\emptyset'$ (°)	25	27	27	28	33	28	28	36
Ψ' (°)	0	0	0	0	5	0	0	5
E_{oed}^{ref} (MPa)	45.6	5	20	60	80	60	60	80
E_{50}^{ref} (MPa)	45.6	5	20	60	80	60	60	80
E_{ur}^{ref} (MPa)	136.8	15	100	180	240	180	180	240
v_{ur}	0.2	0.2	0.2	0.2	0.2	0.2	0.2	0.2
m	1	1	1	1	0.5	1	1	0.5
K_0^{nc}	0.58	0.6	0.6	0.5	0.55	0.5	0.5	0.5
R_f	0.9	0.9	0.9	0.9	0.9	0.9	0.9	0.9
G_{max} (MPa)	-	15	45	80	200	80	130	240
$\gamma_{0.7}$	-	0.08	0.11	0.12	0.014	0.12	0.15	0.02
Analysis type	Drained	Undrained	Undrained	Undrained	Undrained	Undrained	Undrained	Undrained

are three strain components (*x*-, *y*- and *z*-directions). In tunneling simulation, CR was used to reconcile the simulated and measured ground surface settlement (i.e., making both agreeable), and VS was to regularize the lining force (bending moment and axial force).

The linearly increasing face pressure at the tunnel crown and invert of 150 and 200 kPa, respectively, and the grouting pressure of 200 kPa. The simulations were carried out using earth pressure balance (EPB) tunneling method. Data on the tunnel construction and field measurement of CS-8C section of the Blue Line subway project of the Metropolitan Rapid Transit (MRT) in Thailand's capital Bangkok (i.e., measured data) were used in the tunneling simulation (Suwansawat and Einstein 2002). The properties of EPB shield and solid grout were from Katebi *et al.* (2015) and Kasper and Meschke (2004, 2006), respectively

In the 3D full models (models 1-2), the EPB tunneling consisted of four steps (Steps 1-4). Steps 1-3 follow Lueprasert *et al.* (2017b) with minor modifications, and VS was applied to the grouting layer in Step 4, as illustrated in Fig. 1(a). In the 3D symmetry (models 3-4) and 2D models (models 5-8), in the tunneling step (Step 1), the soil elements in the tunneling zone were deactivated and the EPB shield was activated with CR. In Step 2, EPB shield was deactivated and the grouting pressure (200 kPa) applied to the excavated soil periphery. The grouting pressure was removed, meanwhile tunnel lining and grouting layer were incorporated in Step 3. In step 4, VS (for each analysis method) was applied to the grouting layer for adjusting the computed lining forces to be in the practical range and approximately the same.

2.2 Loaded pile simulation

In loaded pile row simulation, simulations were performed with two pile types: volume pile and embedded pile. The simulations were carried out with a pile row in the 3D full models with volume pile (model 1) and embedded pile (model 2); with a single pile in the 3D symmetry models with volume pile (model 3) and embedded pile (model 4); and with a pile wall in the 2D models with volume pile (models 5-7) and embedded pile (model 8). To ensure the ideal pile row condition, preliminary analyses have been carried out and the sufficient numbers of piles in a row is 13 for pile spacing (*S*) of 3, 4 and 6 m and 17 for *S* of 2 m in the 3D full models (models 1-2) to eliminate the

edge effect (Heama *et al.* 2017).

In 2D loaded pile wall simulation, three transformation methods were used to convert 3D pile row (in model 1) into 2D pile wall: equivalent dimensions (model 5), equivalent axial rigidity (model 6), and equivalent flexural rigidity (model 7). Table 1 tabulates the 3D and 2D simulation models under study (i.e., models 1-8).

The wished-in-place loaded pile row was modeled on one side of the existing tunnel. The total displacement was reset to zero, and thus only the tunnel deformation attributable to adjacent loaded pile row was evaluated. The working load was 40 % of the ultimate pile capacity determined by α-method (Skempton 1959).

In the 3D simulation with loaded volume pile (models 1 and 3), the actual pile dimension (i.e., diameter and length) and pile properties were used. For loaded embedded pile (models 2 and 4), an embedded beam element was used for the loaded pile. The input parameters of the embedded beam were diameter (D), unit weight (γ), Poisson's ratio (v), and Young's modulus (E). In the simulation, the unit weight of the loaded embedded pile ($\gamma_{embedded}$) was subtracted by the unit weight of soil (Tschuchnigg and Schweiger 2015).

In the 2D loaded embedded pile row (model 8), the input parameters were the actual pile dimension and pile properties. The actual values were converted into those of embedded pile row which was spread out over the out-of-plane spacing of the pile, as expressed in Eqs. (2)-(4) (Sluis *et al.* 2014)

$$E_{embedded}=E_{pile}\frac{A}{h_{eq}S} \tag{2}$$

$$\gamma_{embedded}=\gamma_{pile}\frac{A}{S} \tag{3}$$

with

$$h_{eq}=\sqrt{\frac{12I}{A}} \tag{4}$$

where A and S are the area and pile spacing, respectively, I is moment of inertia of pile, γ_{pile} is unit weight of pile, and h_{eq} is a radius of half the equivalent pile width.

3. Finite element simulation of pile-soil-tunnel interaction

3.1 Characteristics of tunnel, piles, and soil profile

In Fig. 2, the lining thickness (T), outer diameter (D_{tunnel}), and tunnel depth (Z_{tunnel}) at the CS-8C section of the existing subway tunnel were 0.3 m, 6.3 m, and 20.5 m, respectively. The diameter of loaded pile (D_{pile}) was 1 m and the edge-to-edge clearance (C) was 0.5 m. The pile spacing (S) was varied between 2, 3, 4, and 6 m, and the positions of pile tip or pile length (Z_{pile}) were 17.35 m (short pile) and 57.0 m (long pile).

Fig. 3 shows the soil profile at the CS-8C section, consisting of made ground at 0–2.5 m; soft clay at 2.5–12 m; medium clay at 12–14 m; 1st stiff clay at 14–20 m; 1st clayey sand at 20-21.5 m; 2nd stiff clay at 21.5-26.5 m; hard clay at 26.5-54 m; and 2nd clayed sand at 54–80 m. A typical pore water pressure profile in Bangkok is a piezometric drawdown as shown in Fig. 3. This is due to the over pumping of the ground water in the past.

Table 3 Material properties of the 3D and 2D FE simulation models

	Young's modulus (E, kN/m^2)	Poisson's ratio (v)	Unit weight (γ, kN/m^3)
Tunnel lining	31 x 10^6	0.20	24
Loaded pile	31 x 10^6	0.20	24
EPB shield	210 x 10^6	0.28	78
Grouting layer	1 x 10^6	0.30	21

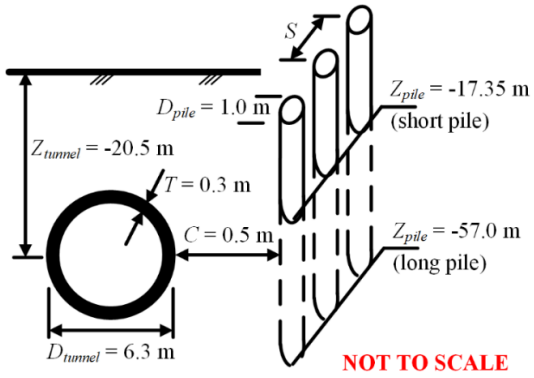

Fig. 2 Geometric parameters in the modeling of pile-tunnel interaction

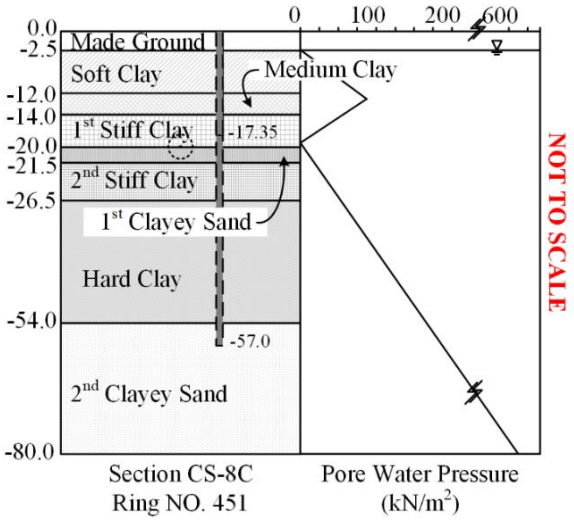

Fig. 3 Soil profile at section CS-8C of the Blue Line subway project and corresponding groundwater

3.2 3D and 2D simulation models and material properties

In the 3D and 2D simulation models, the hardening soil model with small-strain stiffness (HSS) was used to simulate the soil layers below made ground, and the hardening soil model (HSM) was to simulate the made ground layer. Table 2 presents the parameters of soil profile in Bangkok. The

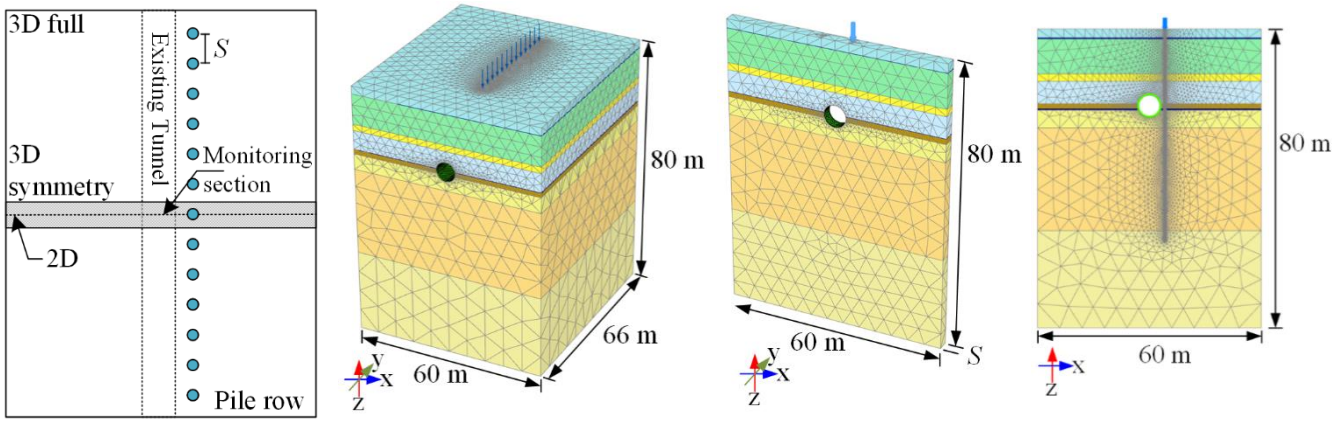

(a) Top view of models 1-8 (b) 3D full (models 1-2) (c) 3D symmetry (models 3-4) (d) 2D models (models 5-8)

Fig. 4 Boundary and FE mesh of existing tunnel with adjacent loaded pile row

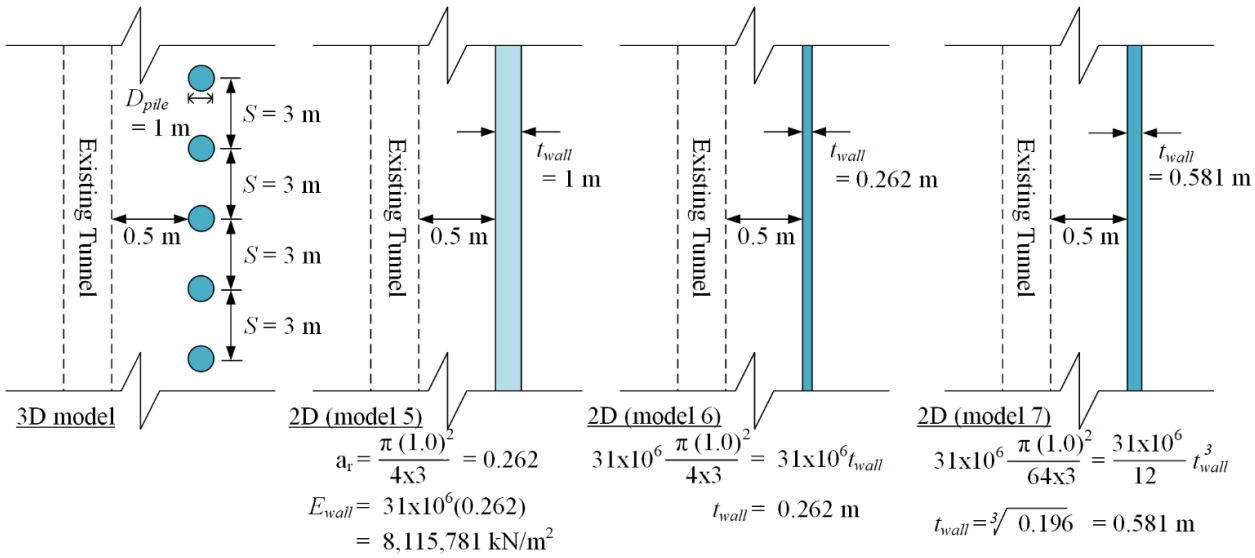

Fig. 5 Conversion 3D loaded pile row into 2D equivalent pile wall for models 5, 6, and 7, given S = 3 m

parameters are adopted from previous study (Likitlersuang *et al.* 2013, Waichita *et al.* 2019), which were calibrated from comprehensive soil testing and in-situ tests in the past projects.

Table 3 tabulates the material properties, including the tunnel lining, loaded pile, EPB shield, and grouting layer modeled as linear elastic material. The interface friction (R_{inter}) between the structural elements (tunnel lining, loaded piles, and EPB) and surrounding soil is 0.9 as suggested in previous research (Brinkgreve *et al.* 2018a; Lueprasert *et al.,* 2017a; Mathew and Lehane 2012).

The soil profile and grouting layer were discretized into 15-node triangular elements in 2D FEA and 10-node tetrahedral elements in 3D FEA. The loaded volume pile was discretized into 15-node triangular elements in 2D FEA and 10-node tetrahedral elements in 3D FEA; and into 5-node beam elements in 2D FEA and 3-node beam elements in 3D FEA for the loaded embedded pile. The tunnel lining and EPB shield were discretized into 5-node beam elements in 2D FEA and 6-node triangular plate elements in 3D FEA (Brinkgreve *et al.* 2018a, b).

The interface stiffness factors (*ISF*) of simulated 2D embedded pile row (model 8), including the axial skin stiffness factor (ISF_{RS}), lateral stiffness factor (ISF_{RN}), and pile base stiffness factor (ISF_{KF}) are a function of out-of-plane pile spacing. The calculation of *ISF* uses the stiffness functions as developed by Sluis *et al.* (2014). However, The *ISF* could be overridden by users to match the pile displacement (Sluis *et al.* 2014). The final values used in this study are 0.85, 0.85, and 8.5, respectively.

3.3 3D and 2D simulation models

3.3.1 3D finite element modeling

Fig. 4(a) illustrates the top view of the boundaries of 3D full models (models 1-2), 3D symmetry models (models 3-4), 2D models (models 5-8), and the monitoring section, given the edge-to-edge clearance (C) of 0.5 m. In 3D FE modeling (models 1-2), the minimum model boundary in longitudinal direction was $4.0D_{tunnel}$ each in the front and rear of the monitoring section and was $3.5D_{tunnel}$ in

lateral direction from either side of the tunnel edge (Mroueh and Shahrour 2002). In this research, the 3D model boundaries were $5.5D_{tunnel}$ in longitudinal direction and $4.25D_{tunnel}$ in lateral direction. The boundary dimensions were 60 m in width, 66 m in length, and 80 m in height (Fig. 4(b)).

In Figs. 4(b) and 4(c), the lateral displacements at vertical side of the 3D full models (models 1-2) and 3D symmetry models permitted. The lateral and vertical displacements at the (models 3-4) were fixed, while the vertical displacement was bottom boundary were fixed. To improve accuracy, finer meshes were generated in the zone around the tunnel and loaded pile. The total numbers of elements and nodes for the 3D full models (models 1-2) were approximately 550,000 and 620,000, respectively (Fig. 4(b)).

Fig. 4(c) depicts the cross-sectional area of the 3D symmetry models (models 3-4) whose strip thickness was the center-to-center pile spacing (S). The total numbers of elements and nodes were approximately 27,000 and 39,000, respectively. The loaded piles of either volume pile or embedded pile type were lined on one side of the existing tunnel.

3.3.2 2D finite element modeling

Fig. 4(d) shows the 2D simulation model (models 5-8) whose width and height were 60 and 80 m, respectively, identical to the 3D models (models 1-4). The lateral displacement at the left and right sides of model was fixed, while the vertical displacement was permitted. The lateral and vertical displacements at the bottom boundary were fixed.

The 3D loaded pile row was converted into 2D equivalent pile wall under plane strain condition. Fig. 5 illustrates the conversion of 3D loaded pile row into 2D pile wall by using equivalent dimensions (model 5), equivalent axial rigidity (model 6), and equivalent flexural rigidity (model 7), given S = 3 m.

In the equivalent dimensions (model 5), the 2D wall width (t_{wall}) was identical to the 3D loaded pile diameter (D_{pile}). The equivalent elastic modulus of the pile wall (E_{wall}) is the summation of average area-weighted of the loaded pile properties and soil between loaded piles, as shown in Eq. (5).

$$E_{wall}=E_{pile}a_r+E_{soil}(1-a_r) \quad (5)$$

where E_{pile} and E_{soil} are the elastic moduli of actual loaded pile and soil, respectively, and a_r is the improvement area resulting from the loaded pile. In this research, E_{pile} was substantially larger than E_{soil}, so E_{soil} was ignored in Eq. (1).

In models 6-7, since the properties of pile wall (E_{wall}) were identical to those of actual loaded pile (E_{pile}), the width of the pile wall (t_{wall}) was thus unequal to the diameter of actual loaded pile (D_{pile}). The width of pile wall under plane strain conditions (t_{wall}) based on equivalent axial rigidity and flexural rigidity could be calculated by Eqs. (6)-(7), respectively.

$$E_{pile}\left(\frac{\pi D_{pile}^2}{4S}\right)=E_{wall}t_{wall} \quad (6)$$

Table 4 Parameters of 2D loaded pile wall under plane strain condition

Pile spacing (S)	Model 5		Model 6	Model 7
	a_r	E_{wall} (kN/m^2)	t_{wall} (m)	t_{wall} (m)
S = 2 m	0.393	12,179,671	0.393	0.665
S = 3 m	0.262	8,115,781	0.262	0.581
S = 4 m	0.196	6,086,836	0.196	0.528
S = 6 m	0.131	4,057,891	0.131	0.461

Table 5 The contraction ratio (CR) of EPB shield and volumetric strain (VS) of grouting layer in tunneling simulation

Model	CR	VS
3D full (models 1-2)	0.3%	3.5%
3D symmetry (models 3-4)	0.5%	4.0%
2D plane strain (models 5-8)	0.5%	9.5%

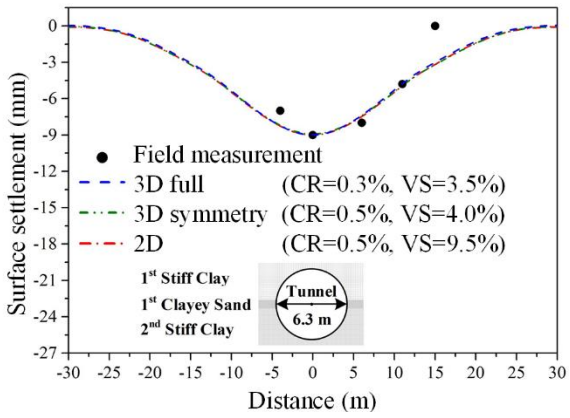

Fig. 6 Simulated ground surface settlement of 3D full (models 1-2), 3D symmetry (models 3-4), 2D models (models 5-8) in comparison with the measured ground surface settlement of section CS-8C of the Blue Line subway project

$$E_{pile}\left(\frac{\pi D_{pile}^2}{64S}\right)=E_{wall}\left(\frac{1}{12}t_{wall}^3\right) \quad (7)$$

where E_{pile} and E_{wall} are the elastic moduli of actual loaded pile and pile wall, respectively, and S is the center-to-center loaded pile spacing.

Table 4 tabulates the parameters of 2D loaded pile wall under plane strain condition (models 5-7). The working stress on pile wall (P_{wall}) was calculated by dividing the working load of single pile (P_{pile}) by the width of the pile wall (t_{wall}) times out-of-plane spacing of pile (S), as expressed in Eq. (8) (Ukritchon *et al.* 2016).

$$P_{wall}=\left(\frac{P_{pile}}{t_{wall}S}\right) \quad (8)$$

3.4 Validation of simulation models

3.4.1 Tunneling simulation validation

To evaluate the performance of models 1-8 in

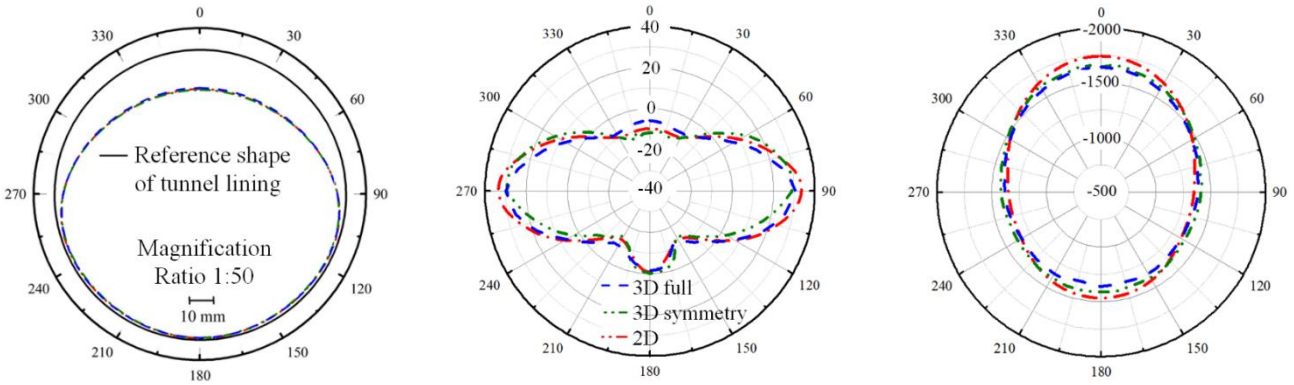

(a) Tunnel deformation (b) Bending moment (c) Axial force

Fig. 7 The simulated tunnel responses as a result of tunneling in circumferential direction

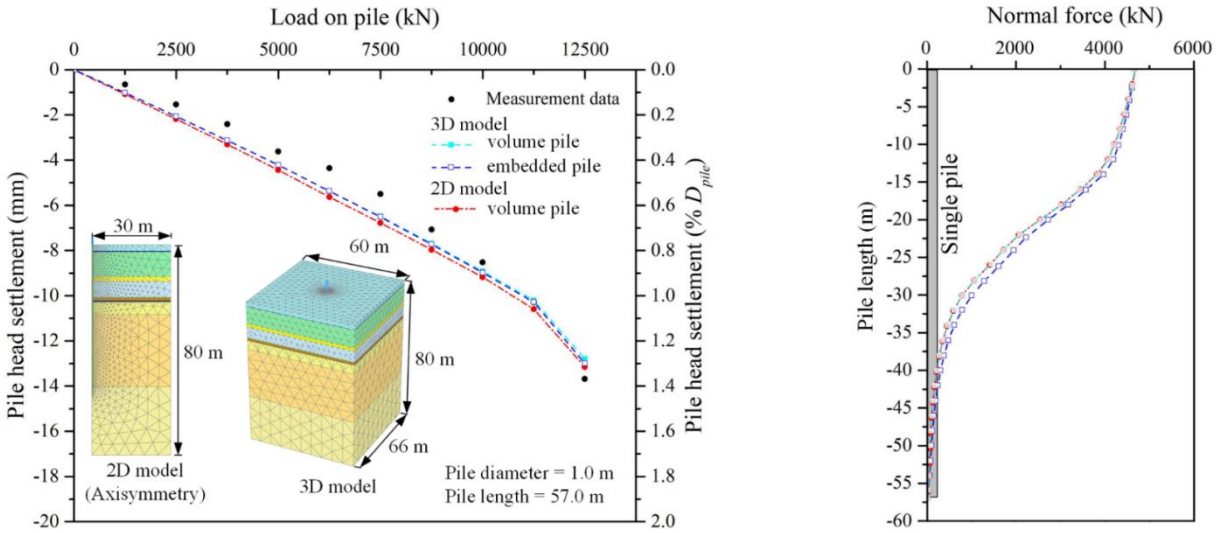

(a) Simulated pile head settlements vis-à-vis static pile load test (b) Normal force along pile length

Fig. 8 Loaded single pile simulation of 3D and 2D models (models 1-8)

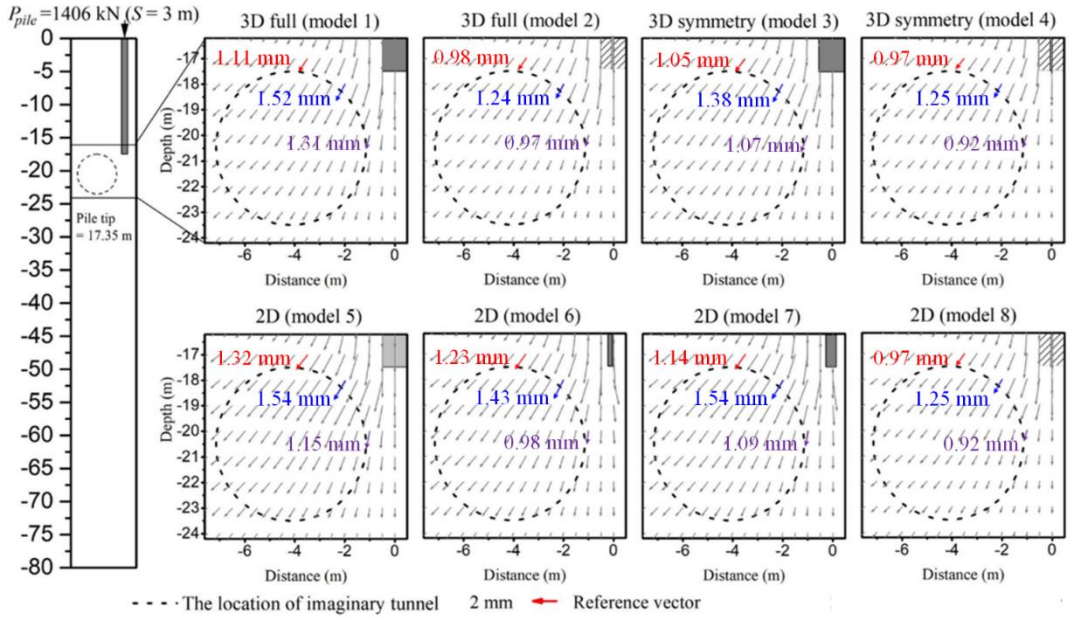

Fig. 9 Simulated vectors of soil displacement near the loaded pile row at the monitoring section (without tunnel), given S = 3 m, 17.35 m pile length, and 1406 kN working load on pile (40% of ultimate load capacity)

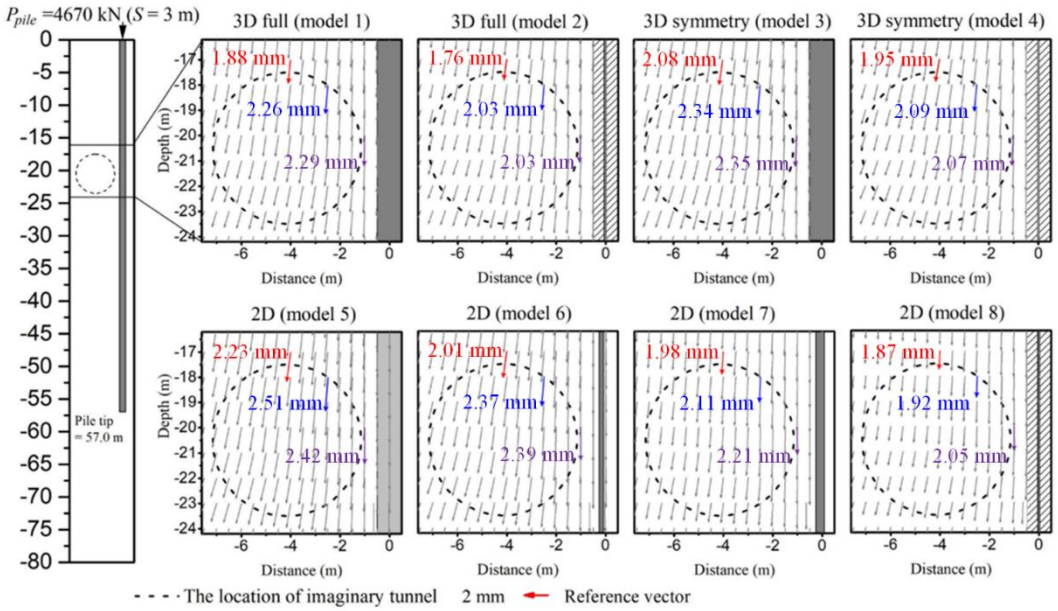

Fig. 10 Simulated vectors of soil displacement near the loaded pile row at the monitoring section (without tunnel), given S = 3 m, 57.0 m pile length, and 4670 kN working load on pile (40% of ultimate load capacity)

tunneling simulation, the simulated ground surface settlements were validated against the measured ground surface settlement of CS-8C section of the subway project. Simulations were carried out by varying contraction ratio (CR) of the EPB shield and volumetric strain (VS) of the grouting layer.

Table 5 tabulates the CR and VS in tunneling simulation of models 1-8. The CR and VS of 3D full models (models 1-2) were smallest (0.3 % and 3.5 %), followed by those of 3D symmetry models (models 3-4; 0.5 % and 4.0 %) and the 2D models (models 5-8; 0.5 % and 9.5 %). It is seen that both the CR and VS values in models 3-8 are greater than models 1-2. A similar tendency was found in previous study of the tunneling works (Mathew and Lehane 2013, Zhao *et al.* 2019).

The results were attributable to the exclusion of face pressure

in the 3D symmetry and 2D models (models 3-8) and different numbers of strain components between 2D and 3D models.

Fig. 6 compares the simulated and measured ground surface settlements, and the simulated and measured results were in good agreement. Figs. 7(a)-7(c) respectively illustrate the simulated tunnel responses as a result of tunneling in circumferential direction in terms of tunnel deformation (1:50 magnification ratio), bending moment (M), and axial force (N).

3.4.2 Loaded-pile simulation validation

To assess the performance of pile and soil properties in 3D and 2D FE models, the simulated single-pile head settlements were validated against the static pile load test of a 32-storey residential complex. Since there were no large structures or buildings at or near the CS-8C section, this research used the 32-storey residential complex which is located approximately 200 m away. Axial symmetry

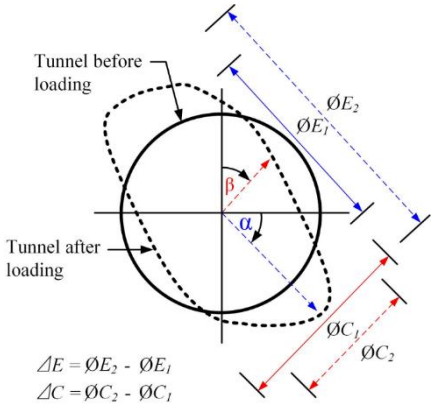

Fig. 11 Out-of-roundness tunnel deformation with respect to maximum extension change (ΔE) and maximum contraction change (ΔC)

boundary conditions were used to simulate the single pile in the 2D models.

Fig. 8(a) compares the simulated pile head settlements of 3D and 2D FE models against the static pile load test and the results were generally agreeable. Fig. 8(b) compares the simulated normal force along pile length of 3D and 2D FE models, given the pile diameter and length of 1 m and 57.0 m, respectively. This indicates that the pile and soil properties can be used to subsequently investigate the effects of adjacent loaded pile row on existing tunnel in models 1-8. Noted that the pile head settlement of 17.35 m pile length (short pile) was not simulated due to the unavailability of data on the static pile load test of the short pile.

3.5 Soil displacement simulation

Fig. 9 compares the simulated vectors of soil

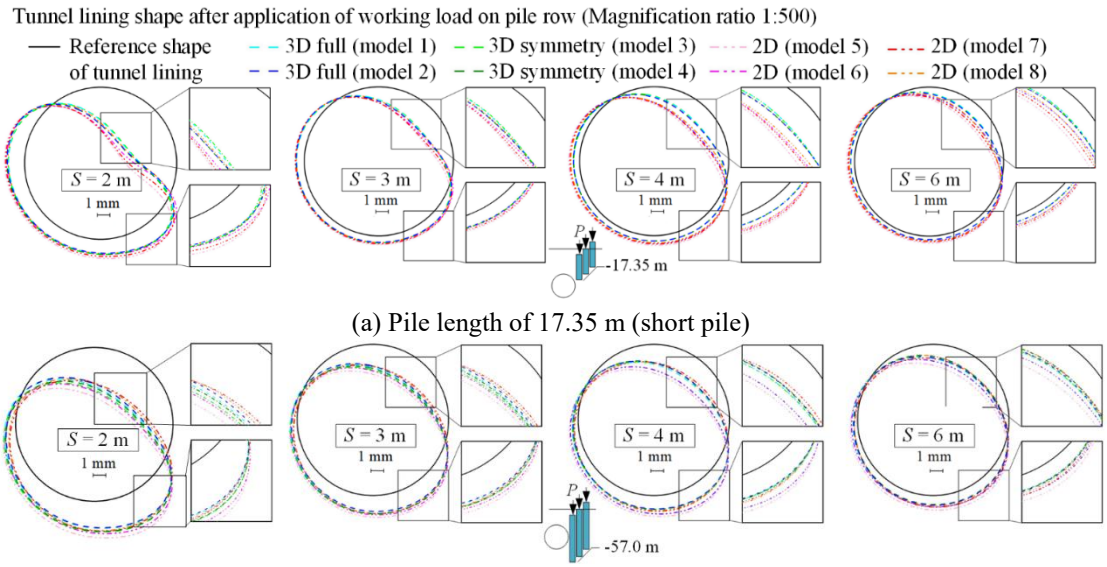

(a) Pile length of 17.35 m (short pile)

(b) Pile length of 57.0 m (long pile)

Fig. 12 Simulated tunnel deformation as a result of adjacent loaded pile row of models 1-8

displacement (without tunnel) near the loaded pile row at the monitoring section (Fig. 4(a)), given S = 3 m, 17.35 m pile length, and 1406 kN working load on pile (40 % of ultimate load capacity). Fig. 10 shows those of 57.0 m pile length and 4670 kN working load on pile (without tunnel). The vectors indicated the relative magnitude and direction of soil displacement with a magnification ratio of 1:500. The dotted circle was used to indicate the location of imaginary tunnel. To accommodate the comparison among different analysis methods, three vectors of soil displacement at the top, upper right, and right side of the dotted circle were traced and highlighted with red, blue and, purple.

In Fig. 9, the vector magnitude became smaller with increase in distance from the pile tip (17.35 m) with the soil vector (vector direction) moving diagonally. In Fig. 10, the vector magnitude became smaller as the distance from the long pile (57.0 m) increased, with the soil vector moving downward. The vector magnitude of soil displacement was inversely correlated to the pile spacing (S = 2, 3, 4, and 6 m), while the vector direction remained unchanged, independent of the pile spacing. The simulation results revealed the similarity in soil displacement around the location of tunnel of models 1-8 (Figs. 9 and 10), although slightly smaller and greater soil displacement can be seen in models with embedded piles (models 2, 4 and 8) and models 5 and 6, respectively. The tunnel response was directly related to the soil displacement around the tunnel with loaded single pile (Lueprasert *et al.* 2017a).

4. Simulation results and discussion

4.1 Effect of adjacent loaded pile row on tunnel response

In this research, the tunnel response of adjacent loaded pile row included tunnel deformation and lining force. Due to unsymmetrical tunnel deformation as a result of the loaded pile row on one side of the tunnel, the out-of-roundness method was used to determine the maximum tunnel deformation (Gillie 2011).

Fig. 11 illustrates the out-of-roundness tunnel deformation with respect to maximum extension change (ΔE) and maximum contraction change (ΔC), where α and β represent the maximum extension and contraction degrees. In this research, the tunnel deformation was attributed to evaluate only the effect of adjacent loaded pile row, excluding the tunnel deformation due to tunneling (i.e., zero total displacement). However, the lining force (bending moment and axial force) belonged to tunneling and the adjacent loaded pile row.

4.1.1 Tunnel deformation

The tunnel deforms as a kidney or ellipse shape when the loaded pile row is located at one side of the tunnel. This tunnel deformed shape is also documented in previous works of tunnels due to nearby construction of a new structure (Lin *et al.* 2019, Lueprasert *et al.* 2017a, Zheng *et al.* 2020). Figs. 12(a) and 12(b) compare the effect of adjacent loaded pile row on tunnel deformation of models 1-8, with 17.35 m (short) and 57.0 m (long) pile length, respectively, given S of 2, 3, 4, and 6 m. In Fig. 12(a) (short pile), the tunnel deformation was most pronounced in the upper tunnel spring line adjacent to the loaded pile row. The tunnel invert also experienced small deformation. In Fig. 12(b) (long pile), the upper tunnel spring line adjacent to the loaded pile row and the tunnel invert suffered tunnel deformation. Similar tunnel deformation as a result of adjacent loaded single pile, but with smaller magnitude, was reported in Lueprasert *et al.* (2017a).

Under short pile condition, given the same S, the tunnel deformation was similar for models 1-8, although some discrepancies can be seen from 2D models, particularly models 5 and 6. Considering the soil displacement illustrated in Fig. 9, it seems that the tunnel deformation is

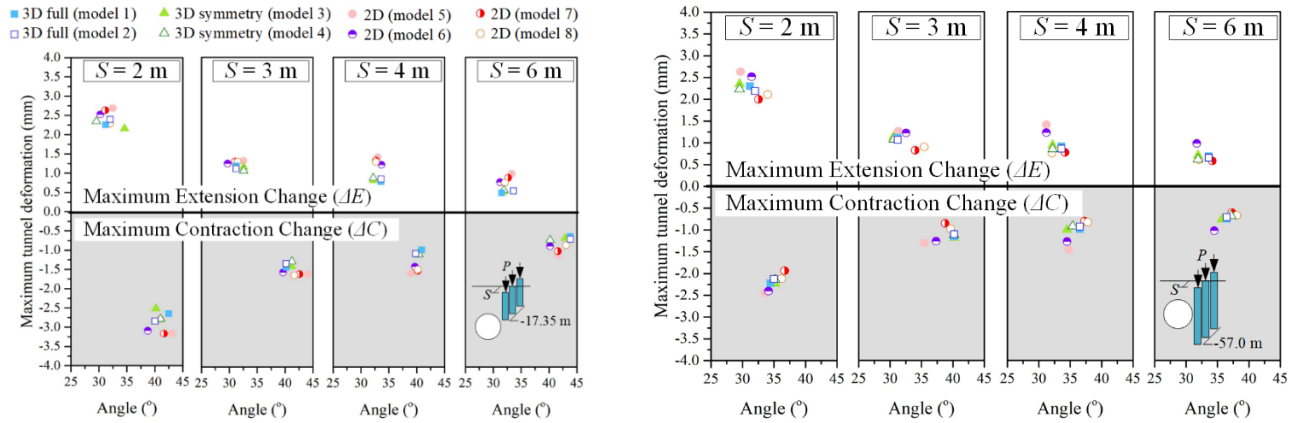

(a) Pile length of 17.35 m (short pile) (b) Pile length of 57.0 m (long pile)

Fig. 13 Simulated maximum tunnel deformation of models 1-8

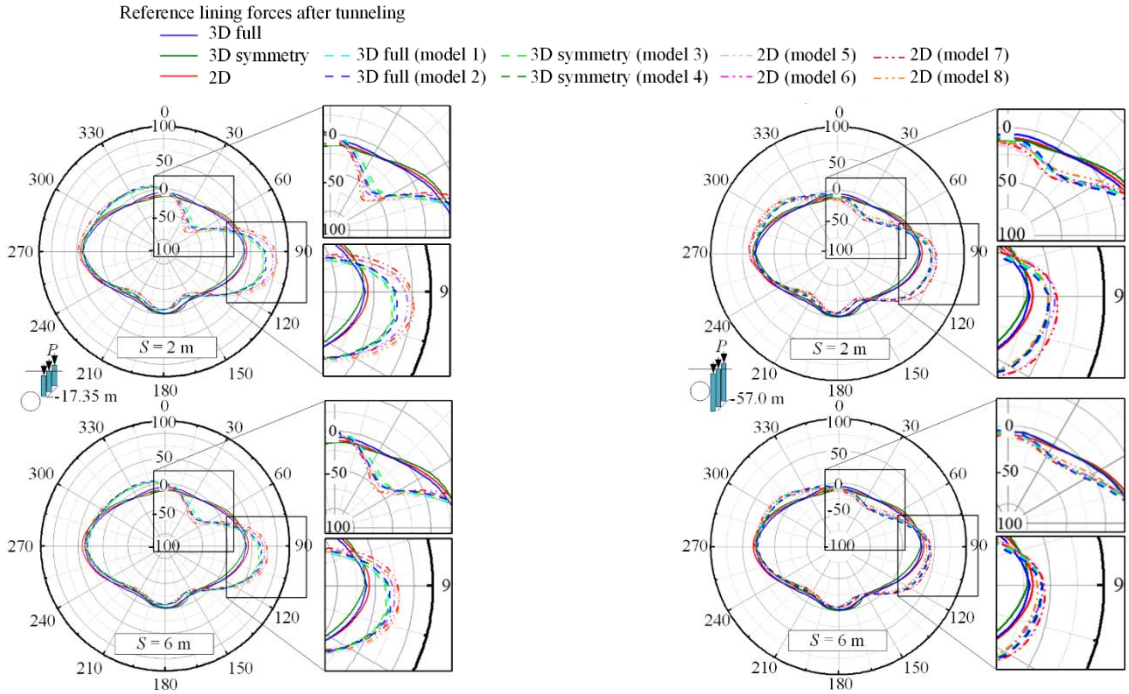

(a) Pile length of 17.35 m (short pile) (b) Pile length of 57.0 m (long pile)

Fig. 14 Simulated bending moment (kNm/m) as a result of adjacent loaded pile row of models 1-8

related to soil displacement in the vicinity of the tunnel crown. Under long pile condition with the same S, the tunnel deformation of 2D models (models 5-6) was also larger than that of 3D full (models 1-2) and 3D symmetry models (models 3-4). For this condition, the soil deformation of the entire zone between the tunnel and the pile affects the tunnel deformation. This supports that the pile-soil-tunnel interaction is principally governed by the soil movement behavior.

Figs. 13(a)-(b) show the simulated maximum tunnel deformation ΔE and ΔC against the maximum extension (α) and contraction (β) degrees, respectively, in which the tunnel translation was excluded. Fig. 13 depicts the results of models 1-8, with 17.35 m and 57.0 m pile length, respectively, given S = 2, 3, 4, and 6 m. In this research, ΔE was positive and ΔC was negative. The ΔE and ΔC in all 3D models (models 1-4), were almost identical, indicating the effectiveness of using the symmetry model to reduce the calculation effort and time of full 3D model. For short pile condition (Fig. 13(a)), the ΔE and ΔC of 2D models (models 5-8) were slightly larger than those of 3D models. In contrast, for long pile condition (Fig. 13(b)), ΔE and ΔC of only models 5 and 6 were slightly greater than those of 3D models. By comparing each pair of analyses using the same modeling technique but different pile type in 3D models (i.e., model 1 and 2; model 3 and 4), the loaded pile types (volume pile and embedded pile) had minimal impact on the maximum tunnel deformation (ΔE and ΔC). For 2D models, ΔE and ΔC of model 8 (modeling with embedded pile row) were close to those of model 7

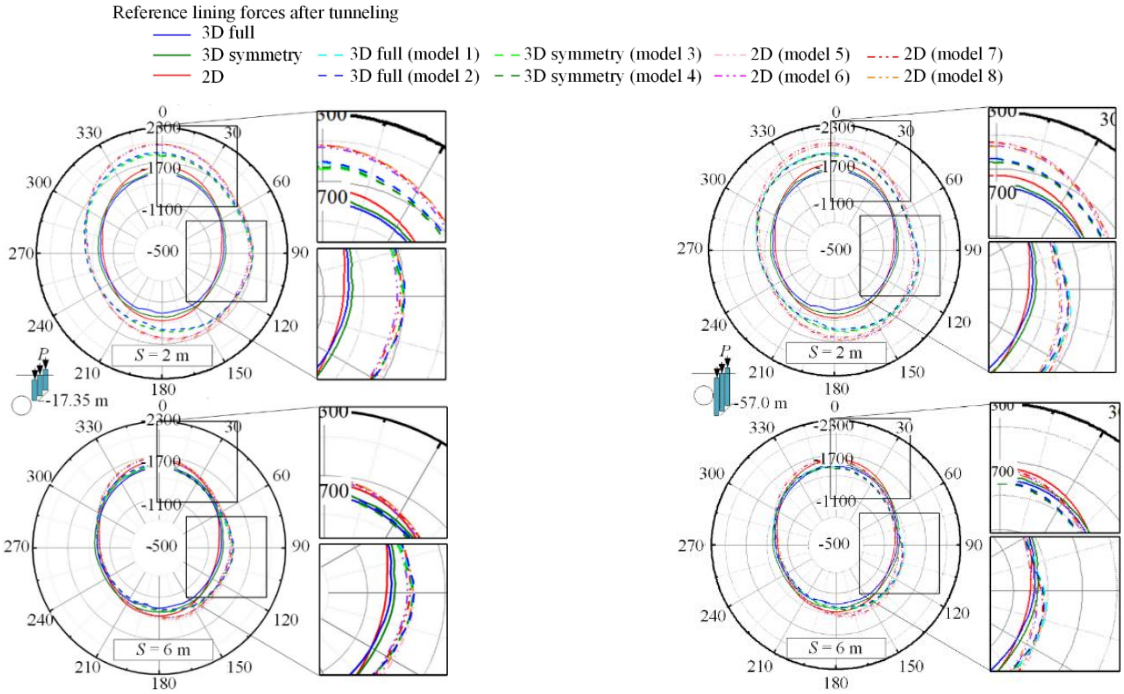

(a) Pile length of 17.35 m (short pile) (b) Pile length of 57.0 m (long pile)

Fig. 15 Simulated axial force (kN/m) as a result of adjacent loaded pile row of models 1-8

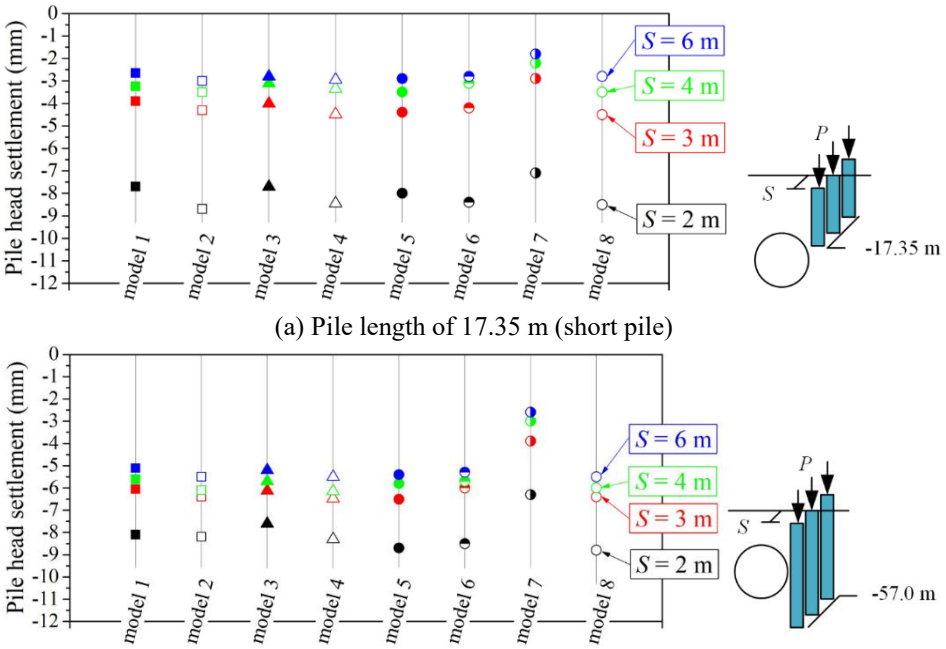

(a) Pile length of 17.35 m (short pile)

(b) Pile length of 57.0 m (long pile)

Fig. 16 Simulated pile head settlement at the monitoring section of models 1-8

(equivalent flexural rigidity). This is attributed to the fact that the flexural rigidity is also considered in the formulation of embedded pile element. It is indicated that the mechanism behind the pile-soil-tunnel interaction is governed by pile axial behavior, not the flexural one. In the viewpoint of engineering practice, models 5 and 6 are thus recommended since they provide conservative estimation.

By further investigating the simulated vectors of soil displacement (without tunnel) near the loaded pile row at the monitoring section for cases with all pile spacings, such as the cases with S = 3 m as shown in Figs. 9 and 10, it is evident that if the main mechanism of soil displacement induced by adjacent loaded pile row can be sufficiently well reproduced, any simulation models can be adopted to evaluate the tunnel deformation, which in turn depend on the adjacent loaded pile row behaviour.

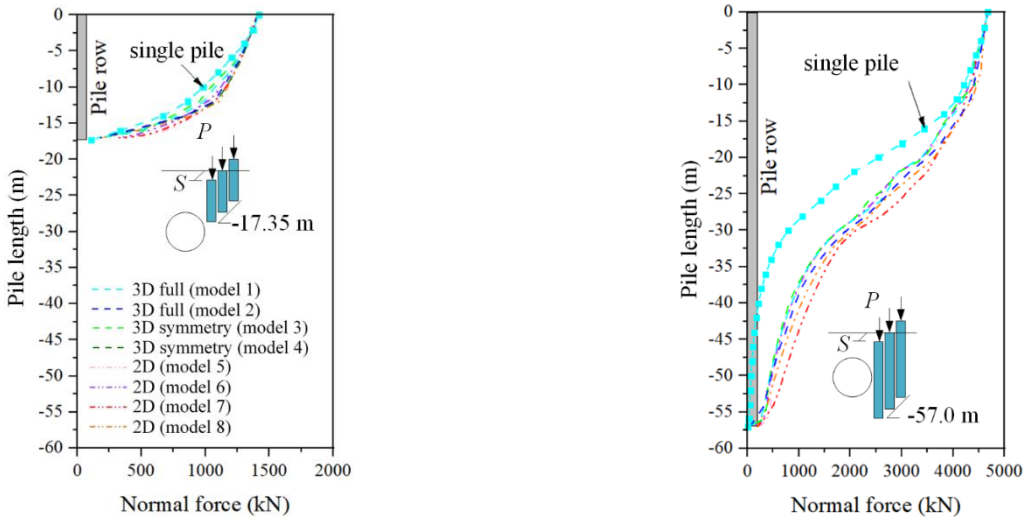

(a) Pile length of 17.35 m (short pile) (b) Pile length of 57.0 m (long pile)

Fig. 17 Simulated normal force along pile length at the monitoring section of models 1-8, given S = 3 m

4.1.2 Lining force

Figs. 14(a) and 14(b) illustrate the simulated bending moment (M) in circumferential direction due to adjacent loaded pile row of models 1-8, with the short (17.35 m) and long (57.0 m) piles, respectively, given S of 2 and 6 m. The origin (θ = 0°) was at the tunnel crown. In the figure, the solid lines represent the tunneling-induced bending moment (reference), and the dashed lines the bending moments of models 1-8.

The bending moment changed significantly relative to the reference (tunneling-induced bending moment) in the range of θ = 300° to 0° and 0° to 120° for both short and long piles. The maximum positive and negative bending moments were at θ of approximately 45° and 105° for the short pile and approximately 37° and 120° for the long pile, corresponding to the maximum α and β. By comparison, the changes in bending moment under the short pile condition were more pronounced than under the long pile condition. It is seen from the figure that the simulated bending moments were almost identical among 3D models (models 1-4). The bending moments in models 5-8 (2D models) were also similar to each other but larger than those of 3D models. The differences between bending moments in 3D models and 2D models become significant for cases with small pile spacing (S = 2 m). Note also that the reference bending moment (from tunneling) in 2D model was slightly greater than those of 3D models.

Figs. 15(a) and 15(b) illustrate the simulated axial force (N) in circumferential direction due to adjacent loaded pile row of models 1-8, with the short (17.35 m) and long (57.0 m) piles, respectively, given S of 2 and 6 m as examples. The changes in axial force closely resembled the changes in bending moment under both short and long pile conditions. However, the lining forces in 2D models were generally larger than those of 3D models. This indicates that the analysis by 2D models provide conservative results.

4.2 Loaded pile row behavior

The load transfer behavior of pile row (or normal force along pile length) induces pile settlement and soil displacement. The soil displacement in turn is responsible for the deformation of existing tunnel adjacent to the loaded pile row.

Figs. 16(a) and 16(b) compare the simulated pile head settlement at the monitoring section of models 1-8 (Fig. 4(a)) for 17.35 m (short) and 57.0 m (long) pile length, respectively, given S of 2, 3, 4, and 6 m. The pile head settlement was inversely correlated to the pile spacing for both short and long piles. This is attributed to the overlapping zone of stresses between the two piles in the row. As a result, the pile settlement increases with decreasing pile spacing (Rao *et al.,* 2011). The pile head settlements of 2D models (models 5, 6 and 8 except for model 7) were slightly greater than those of of 3D models (models 1-4). The lowest pile head settlement belonged to 2D equivalent flexural rigidity model (model 7). Similar observation was also found in analyses of embankment supported by piles (Chai *et al.,* 2015; Jamsawang *et al.,* 2019). The finding was attributable to the largest ratio of axial stiffness to the width of pile wall (t_{wall}).

By comparison, the pile head settlement of the short pile was smaller than that of the long pile due to difference in the working load on pile (1406 kN and 4670 kN for the short and long pile, respectively).

Figs. 17(a) and 17(b) compare the simulated normal force along pile length at the monitoring section of models 1-8 for 17.35 m (short) and 57.0 m (long) pile length, respectively, given S of 3 m. In the figures, the normal force of the single pile was included for comparison purposes. Except for model 7, the normal force along pile length of all the simulation models were similar. Specifically, the normal force along pile length of model 7 was largest, giving rise to smallest pile head settlement and smallest tunnel deformation (Fig. 12). Besides, the normal forces along pile length of volume pile and embedded pile were similar (Tschuchnigg and Schweiger, 2015).

In essence, the normal force along pile length was positively correlated with the tunnel response (tunnel deformation, bending moment, and axial force). More

specifically, higher normal force along pile length resulted in higher pile head settlement and soil displacement, giving rise to larger tunnel response.

5. Conclusions

This research simulated the effects of adjacent loaded pile row on existing tunnel in terms of tunnel deformation and lining force (bending moment and axial force). The behavior of adjacent loaded pile row included pile head settlement and normal force along pile length. The simulations were carried out by Plaxis 2D and 3D software, with sufficient number of piles in a row (17 for S = 2 m and 13 for other cases) using 3D FE full models with volume piles (model 1) and embedded piles (model 2); with a single pile in 3D FE symmetry models with volume pile (model 3) and embedded pile (model 4); and with a pile wall in 2D FE models with volume pile (models 5-7) and embedded pile (model 8). The simulation results were subsequently compared and discussed. In 2D simulation, the 3D pile row was converted into 2D pile wall under plane strain condition using equivalent dimensions (model 5), equivalent axial rigidity (model 6), and equivalent flexural rigidity (model 7). The pile diameter was 1 m, and the pile lengths were, respectively, 17.35 m (short pile) and 57.0 m (long pile). The pile spacing (S) was varied between 2, 3, 4, and 6 m, and the edge-to-edge clearance (C) was 0.5 m. The conclusions are as follows:

- The pile-soil-tunnel interaction is mainly governed by the soil movement behavior, particularly in the zone of tunnel crown, and zone between the tunnel and pile for short and long pile condition, respectively. As long as the nature of problem is ideal pile row whose number of pile in the row is sufficiently large, no matter which analysis method is chosen, the tunnel responses are acceptable if the method can reasonably reproduce the soil movement behavior.
- Essentially, the 3D symmetry and 2D simulation models, all pile spacing, could efficiently be employed to simulate the effect of adjacent loaded pile row on existing tunnel. However, 2D models using equivalent dimensions or equivalent axial rigidity are recommended since they provide conservative estimation on both tunnel deformation and induced lining forces. The 2D model with equivalent flexural rigidity is non-ideal for simulating the effect of adjacent loaded pile row on the existing tunnel if the pile response is of concern.
- The pile type (volume pile and embedded pile) had a negligible impact on the tunnel deformation and lining force.

Although, the advantage of 2D models over 3D models is lower computational resources required, particular attention of various adapting methods to model pile row in 2D models must be given in order to simulate the effect of adjacent loaded pile row on the existing tunnel.

The analysis in this study is based on continuous lining, constant values of percentage of ground loss (CR) and volumetric strain of grouting layer (VS) which are determined from a specific tunnel section and MRT tunnel whose lining was designed in a very conservative manner to fulfill the restrictive serviceability criterion. The future work considering the effects of joints, varying CR and VS and tunnel with thinner lining should be done to extent the scope of study.

Acknowledgments

The authors gratefully acknowledge financial support by the 1D2 Group Co. Ltd., Thailand Research Fund (TRF) and King Mongkut's Institute of Technology Ladkrabang through Grant PHD60I0032 and Grant KREF035001. The support from National Research Council of Thailand (NRCT) and King Mongkut's university of Technology Thonburi under Contract no. NRCT5-RSA63006 and Thailand Science Research and Innovation (TSRI) under Fundamental Fund 2022 (Project: Advanced Construction Towards Thailand 4.0) are also acknowledged.

References

Brinkgreve, R.B., Engin, J.E. and Swolfs, W.M. (2018a), *PLAXIS 3D Version 2018 Manual*.

Brinkgreve, R.B., Kumarswamy, S., Swolfs, W.M., Foria, F., Waterman, D., Chesaru, A. and Bonnier, P.G. (2018b), *PLAXIS 2D Version 2018 Manual.*

Chai, J.C., Shrestha, S., Hino, T., Ding, W.Q., Kamo Y. and Carter, J. (2015), "2D and 3D analyses of an embankment on clay improved by soil-cement columns", *Comput. Geotech.*, **68**, 28-37. https://doi.org/10.1016/j.compgeo. 2015.03.014.

Chen, S.L. and Lee, S.C. (2020), "An investigation on tunnel deformation behavior of expressway tunnels", *Geomech. Eng.*, **21**(2), 215-226. http://doi.org/10.12989/gae.2020. 21.2.215

Djelloul, C., Karech, T., Demagh, R., Limam, O. and Martinez, J. (2018), "2D numerical investigation of twin tunnels-Influence of excavation phase shift", *Geomech. Eng.*, **16**(3), 295-308. http://doi.org/10.12989/gae. 2018.16.3.295

Gillie, M. (2011), "Measures of circularity for shell structures", *J. Struct. Eng.*, **137**, 1241-1243. https:// doi.org/10.1061/(ASCE)ST.1943-541X.0000348.

Heama, N., Jongpradist, P., Lueprasert, P. and Suwansawat, S. (2017), "Investigation on tunnel responses due to adjacent loaded pile by 3D finite element analysis", *Int. J. GEOMATE*, **12**(31), 63-70. https://doi.org/10.21660 /2017.31.6542

Jamsawang, P., Phongphinittana, E., Voottipruex, P., Bergado, D.T. and Jongpradist, P. (2019), "Comparative performances of two- and three-dimensional analyses of soil-cement mixing columns under an embankment load", *Mar. Georesourc. Geotec.*, **37**(7), 852-869. https://doi.org/10.1080/1064119X.2018.1504261

Jeon, Y.J., Jeon, S.C., Jeon, S.J. and Lee, C.J. (2020), "Study on the behaviour of pre-existing single piles to adjacent shield tunnelling by considering the changes in the tunnel face pressures and the locations of the pile tips", *Geomech. Eng.*, **21**(2), 187-200. http://doi.org/10.12989/ gae.2020.21.2.187.

Jongpradist, P., Kaewsri, T., Sawatparnich, A., Suwansawat, S., Youwai, S., Kongkitkul, W. and Sunitsakul, J. (2013), "Development of tunneling influence zones for adjacent pile foundations by numerical analyses", *Tunn. Undergr. Sp. Tech.*, **34**, 96-109. https://doi.org/10.1016/j.tust.2012.11.005.

Kasper, T. and Meschke, G. (2006), "On the influence of face pressure, grouting pressure and TBM design in soft ground tunnelling", *Tunn. Undergr. Sp. Tech.*, **21**, 160-171. https://doi.org/10.1016/j.tust.2005.06.006.

Kasper, T. and Meschke, G. (2004), "A 3D finite element simulation model for TBM tunnelling in soft ground", *Int. J.*

Numer. Anal. Met. Geomech., **28**(14), 1441-1460. https://doi.org/10.1002/nag.395.
Katebi, H., Rezaei, A.H., Hajialilue-Bonab, M. and Tarifard, A. (2015), "Assessment the influence of ground stratification, tunnel and surface buildings specifications on shield tunnel lining loads (by FEM)", *Tunn. Undergr. Sp. Tech.*, **49**, 67-78. https://doi.org/10.1016/j.tust. 2015.04.004.
Klappers, C., Grübl, F. and Ostermeier, B. (2006), "Structural analyses of segmental lining – coupled beam and spring analyses versus 3D-FEM calculations with shell elements", *Tunn. Undergr. Sp. Tech.*, **21**, 254-255. http://doi.org/10.1016/j.tust.2005.12.116.
Likitlersuang, S., Teachavorasinskun, S., Surarak, C., Oh, E. and Balasubramaniam, A. (2013), "Small strain stiffness and stiffness degradation curve of Bangkok Clays", *Soils Found.*, **53**(4), 498-509. https://doi.org/10.1016/j.sandf. 2013.06.003.
Lin, X.T., Chen, R.P., Wu, H.N. and Cheng, H.Z. (2019), "Deformation behaviors of existing tunnels caused by shield tunneling undercrossing with oblique angle", *Tunn. Undergr. Sp. Tech.*, **89**, 78-90. https://doi.org/10. 1016/j.tust.2019.03.021.
Lueprasert, P., Jongpradist, P., Jongpradist, P. and Suwansawat, S. (2017a), "Numerical investigation of tunnel deformation due to adjacent loaded pile and pile-soil-tunnel interaction", *Tunn. Undergr. Sp. Tech.*, **70**, 166-181. https://doi.org/10.1016/j.tust.2017.08.006.
Lueprasert, P., Jonpradist, P. and Suwansawat, S. (2017b), "Tunneling simulation in soft ground using shell elements and grouting layer", *Int. J. GEOMATE.*, **12**(31), 51-57. https://doi.org/10.21660/2017.31.6535.
Mathew, G.V. and Lehane, B.M. (2013), "Numerical back-analyses of greenfield settlement during tunnel boring", *Can. Geotech. J.*, **50**, 145-152. https://doi.org/10.1139/cgj-2011-0358.
Michael, K., Dimitris. L., Ioannis, V. and Petros, F. (2017), "Development of a 3D finite element model for shield EPB tunnelling", *Tunn. Undergr. Sp. Tech.*, **65**, 22-34. http://doi.org/10.1016/j.tust.2017.02.001
Mroueh, H. and Shahrour, I. (2002), "Three-dimensional finite element analysis of the interaction between tunneling and pile foundations", *Int. J. Numer. Anal. Meth. Geomech.*, **26**(3), 217-230. https://doi.org/10.1002/nag.194
Nematollahi, M. and Dias, D. (2019), "Three-dimensional numerical simulation of pile-twin tunnels interaction – Case of the Shiraz subway line", *Tunn. Undergr. Sp. Tech.*, **86**, 75-88. https://doi.org/10.1016/j.tust. 2018.12.002.
Potts, D.M. and Zdravkovic´, L. (1999), *Finite Element Analysis in Geotechnical Engineering: Theory*, Thomas Telford, U.K.
Rao, N.S.V. (2011), *Foundation Design, Theory and Practice*, John Wiley & Sons (Asia) Pte Ltd, 2 Clementi Loop, Singapore.
Schroeder, F.C., Potts, D.M. and Addenbrooke, T.I. (2004), "The influence of pile group loading on existing tunnels", *Geotechnique*, **54**(6), 351-362. https://doi.org/10.1680/geot.2004.54.6.351.
Skempton, A.W. (1959), "Cast in-situ bored piles in London clay", *Géotechnique*, **9**(4), 153-173. https://doi.org/10. 1680/geot.1959.9.4.153.
Sluis, J.J.M., Besseling, F. and Stuurwold, P.H.H. (2014), "Modelling of a pile row in a 2D plane strain FE-analysis", *Proceedings of the 8th European Conference on Numerical Methods in Geotechnical Engineering*, Delft, The Netherlands, June.
Suwansawat, S. and Einstein, H.H. (2002), "Earth pressure balance (EPB) shield tunneling in Bangkok: Ground response and prediction of surface settlements using artificial neural networks", Ph.D. Dissertation, Massachusetts Institute of Technology, Cambridge, Massachusetts, U.S.A.
Tschuchnigg, F. and Schweiger, H.F. (2015), "The embedded pile concept - Verification of an efficient tool for modelling complex deep foundations", *Comput. Geotech.*, **63**, 244-254. https://doi.org/10.1016/j.comp geo. 2014.09.008.
Ukritchon, B., Faustino, J. and Keawsawasvong, S. (2016), "A numerical study of load distribution of pile group foundation by 2D model", *Walailak J. Sci. Technol.*, **13**(8), 669-688.
Vermeer, P.A. and Brinkgreve, R. (1993), "PLAXIS Version 5 Manual", In: Balkema, Rotterdam, Netherlands.
Waichita, S., Jongpradist, P. and Jamsawang, P. (2019), "Characterization of deep cement mixing wall behavior using wall-to excavation shape factor", *Tunn. Undergr. Sp. Technol.*, **83**, 243-253. https:// doi.org/10.1016/j.tust.2018.09.033
Wijerathna, M. and Liyanapathirana, D.S. (2018), "Simplified modelling approaches for DCM column-supported embankments", *Int. J. Geotech. Eng.*, **15**(5), 553-562. https://doi.org/10.1080/19386362.2018.1462023.
Yan, J.Y., Zhang, Z.X., Huang, H.W. and Wang, R.L. (2006), *Numerical Simulation of Interaction between Pile Foundation and Adjacent Tunnel*, in *Underground Construction and Ground Movement*, *American Society of Civil* Engineers, Reston, Virginia, U.S.A. 240-247.
Yoo, C. and Choi, J. (2018), "Effect of construction sequence on three-arch tunnel behavior-Numerical investigation", *Geomech. Eng.*, **15**(3), 911-917. http://doi.org/10.12989/ gae.2018.15.3.911.
Zhang, Z., Huang, M., Xu, C., Jiang, Y. and Wang, W. (2018), "Simplified solution for tunnel-soil-pile interaction in Pasternak's foundation model", *Tunn. Undergr. Sp. Tech.*, **78**, 146-158. https://doi.org/10.1016/j.tust. 2018.04.025.
Zhao, C., Alimardani Lavasan, A. and Schanz, T. (2019), "Application of submodeling technique in numerical modeling of mechanized tunnel excavation", *Int. J. Civ. Eng.*, **17**, 75-89. https://doi.org/10.1007/s40999-018-0318-8.
Zheng, G., Pan, J., Li, Y., Cheng, X., Tan, F., Du, Y. and Li, X. (2020), "Deformation and protection of existing tunnels at an oblique intersection angle to an excavation", *Int. J. Geomech.*, **20**(8), 05020004. https://doi.org/10.1061/(asce)gm.1943-5622.0001766.

JS

Nomenclature

T	lining thickness
D_{tunnel}	outer tunnel diameter
D_{pile}	pile diameter
Z_{tunnel}	tunnel depth
Z_{pile}	pile tip position
S	center-to-center bored pile spacing
C	clearance
γ_{soil}	unit weight of soil
c'	effective cohesion

$\emptyset'$	effective internal friction angle
Ψ'	angle of dilatancy
E_{oed}^{ref}	reference tangent modulus for oedometer primary loading
E_{50}^{ref}	reference secant modulus from drained triaxial test
E_{ur}^{ref}	reference unloading/reloading modulus
v_{ur}	unloading/reloading Poisson's ratio
m	exponential power for modulus
K_0^{nc}	K_0 - value for normal consolidation
R_f	failure ratio
G_{max}	small strain shear modulus
$\gamma_{0.7}$	reference shear strain
γ_{pile}	unit weight of pile
P_{pile}	working load on pile
P_{wall}	working stress on pile wall
a_r	improvement area of pile
t_{wall}	width of the pile wall
E_{wall}	Young's modulus of pile wall
E_{pile}	Young's modulus of actual pile
E_{soil}	Young's modulus of soil
A	area of pile
I	moment of inertia of pile
h_{eq}	radius of half the equivalent pile width
ΔE	maximum extension changes in tunnel diameter
$\emptyset E_1$	tunnel diameter in maximum extension direction before loaded pile
$\emptyset E_2$	tunnel diameter in maximum extension direction after loaded pile
ΔC	maximum contraction changes in tunnel diameter
$\emptyset C_1$	tunnel diameter in maximum contraction direction before loaded pile
$\emptyset C_2$	tunnel diameter in maximum contraction direction after loaded pile